Robotica (2016) volume 34, pp. 1059–1070. © Cambridge University Press 2014
doi:10.1017/S0263574714002057

Realization of foot rotation by breaking the kinematic contact constraint

Xuechao Chen†‡§,*, Qiang Huang†‡§, Zhangguo Yu†‡§, Jing Li†‡§, Gan Ma†‡§, Libo Meng†‡§ and Junyao Gao†‡§

†*Intelligent Robotics Institute, School of Mechatronical Engineering, Beijing Institute of Technology, Beijing, China*
‡*Key Laboratory of Biomimetic Robots and Systems, Ministry of Education, China*
§*Key Laboratory of Intelligent Control and Decision of Complex System, China*

(Accepted July 1, 2014. First published online: July 25, 2014)

SUMMARY
Previous research has revealed that foot rotation of the supporting foot in a single support phase could increase walking speed. This paper presents a method for force-controlled bipeds to realize foot rotation by breaking the kinematic contact constraint between the supporting foot and the ground. An inverse dynamics controller is proposed to make the biped model controllable even when the constraint is broken. In addition, a linear inverted pendulum model is extended to make its ZMP adjustable so that the ZMP can be predefined as required. When the planned ZMP is in the toe, the kinematic contact constraint will be broken and foot rotation can be achieved. A walking simulation demonstrates the effectiveness of the proposed method.

KEYWORDS: Biped robot; Foot rotation; Inverse dynamics; LIPM.

1. Introduction

Because walking has been the fundamental concern in the field of bipedal robots for forty years, researchers have developed many bipedal robots to study this complex nonlinear coupled system, such as ASIMO,[1] HRP-2,[2] BHR,[3] M2V2[4] and PETMAN;[5] and great progress has been made. For an actual robot, the dimension of each limb is fixed, and the motor strength and the moveable range of each joint are limited. These factors often limit walking speed. Enabling a robot to walk faster with these limitations has been the focus of humanoid research.

In 1973, WABOT-1 achieved static walking.[6] It always kept the projection of the Center of Mass (CoM) on the ground within the Supporting Convex Hull (SCH), which seriously restricted walking speed. During the 1990s, researchers developed robots that walked dynamically based on two typical models. The Linear Inverted Pendulum Model (LIPM) and a full-body model based on the Zero Moment Point (ZMP) criterion were used to generate dynamic walking patterns.[7–9] These post 1990 robots usually had their ZMP confined to a small area around the center of the sole in Single Support Phase (SSP) to maintain better stability. It was difficult to rotate the supporting foot around the toe, otherwise the ZMP would shift to the toe and the robot would tip over easily.

In humans, the supporting foot rotates around the toe before the swinging foot contacts the ground in forward walking.[10] In other words, foot rotation occurs in SSP. This feature not only increases stride[11] but also reduces the energy consumed for bipeds,[12] which means it can reduce desired joint torque and moveable range. Therefore, foot rotation is especially beneficial in further increasing walking speed with the existing limitations on joint strength and moveable range.

To imitate human walking, moveable toes were added to the bipeds to produce more human-like walking gaits.[13,14] However, these gaits had foot rotation of the supporting foot after the swinging

* Corresponding author. E-mail: chenxuechao@bit.edu.cn

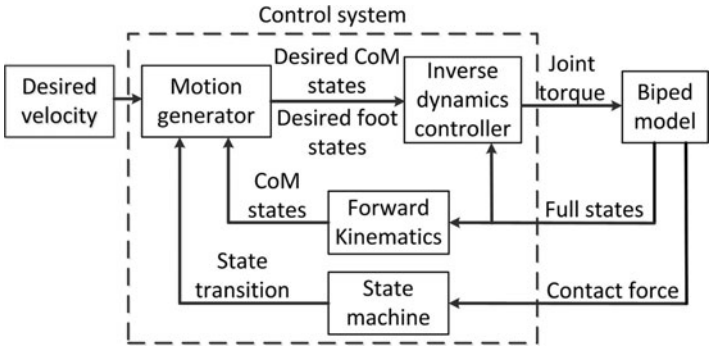

Fig. 1. Control scheme.

foot touched the ground. In fact, foot rotation occurred in Double Support Phase (DSP), which was quite different from human walking. In addition, motion capture systems were used to study human motions, which were then adapted to the robots.[15,16] Due to the great differences between the actors and the robots, the robots could not exactly imitate the actors and foot rotation in SSP was still unrealized.

In summary, the walking described above does not have foot rotation in SSP. A powered robot seldom rotates its supporting foot because it breaks the kinematic contact constraint between the supporting foot and the ground, which is the precondition to derive its whole-body dynamics formulation. If the constraint breaks, the foot would leave the ground unexpectedly and the robot would become an unactuated system. Then, the robot would be quite difficult to control.

This paper presents a method to realize foot rotation by breaking the kinematic contact constraint. An inverse dynamics controller is proposed to make the robot controllable even when the constraint breaks. In addition, LIPM is extended to make its ZMP adjustable, and the ZMP can be predefined into the toe to rotate the supporting foot in SSP.

The rest of this paper is organized as follows. Section 2 introduces the structure of the control system; Section 3 introduces the inverse dynamics controller; Section 4 presents the pattern generator; and the Simulation and Conclusions are provided in Sections 5 and 6, respectively.

2. Structure of Control System

2.1. Control scheme

The control scheme is shown in Fig. 1. The inputs of the control system are desired forward walking velocity, and the full states and contact forces of the biped model. The outputs are joint torques. The full states consist of joint angles, joint velocities, torso position and torso velocity. The contact forces are the Ground Reaction Forces (GRFs).

The control system is composed of three modules: the motion generator, the inverse dynamics controller and the finite state machine. According to the current CoM states and the desired velocity, the motion generator outputs the desired CoM position and velocity, and the desired position and velocity of the swinging foot. The inverse dynamics controller outputs joint torques to track desired trajectories accurately. These two modules are presented in the next two sections in detail. Walking is a rhythmic motion and is divided into six states by finite state machine. Transition occurs according to the time and the contact force.

2.2. Finite state machine

SIMBICON used a finite state machine for walking.[17] To transfer from one state to another more smoothly, two states in DSP are added. Figure 2 shows the finite state machine and its transitions. Transitions occur when a certain amount of time elapses or the swinging foot contacts the ground. When a transition from state 1 to 2 occurs, the robot would lift its left foot as soon as possible if the left foot is still on the ground. When a transition from state 3 to state 4 does not occur after the period of SSP, the robot would put down the left foot as soon as possible so that the transition could

https://doi.org/10.1017/S0263574714002057 Published online by Cambridge University Press

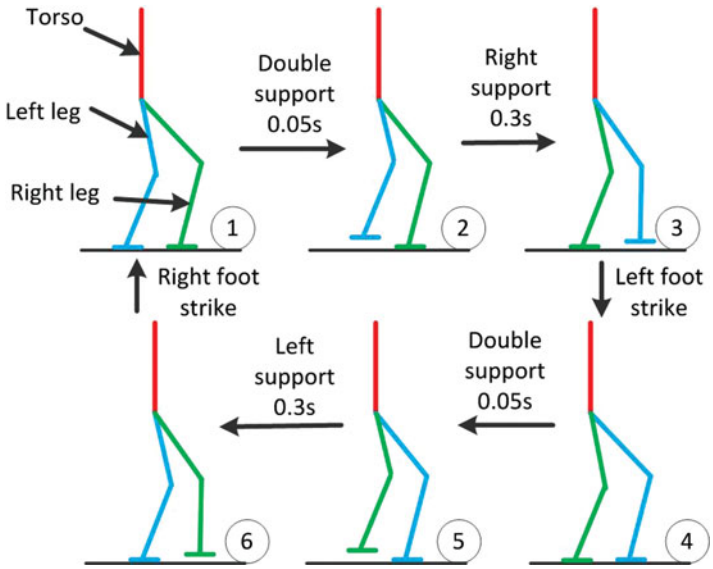

Fig. 2. Finite state machine and its transitions.

happen. A finite state machine is very useful for applying different control policies to different states. For instance, attitude control is used for the supporting leg and landing time control is used for the swinging leg in state 2, 3, 5 and 6, and ZMP control is used in both SSP and DSP.[18]

3. Inverse Dynamics Controller

When deriving the dynamics formulation, we introduce the kinematic constraint, which is due to the contact between the supporting foot and the ground. Only contact between the feet and the ground is considered. The supporting foot is expected to rotate around its toe when the planned ZMP is in the toe, rather than continuously keep its attitude in SSP.

3.1. A bipedal model and its dynamics formulation

As shown in Fig. 3, our biped model has a torso and two legs. Each leg has six joints; so, $q_{rl} \in R^{6\times1}$ and $q_{ll} \in R^{6\times1}$ represent joint angles of the right leg and left leg, respectively. Each foot has a virtual toe, which confines the desired ZMP within it. l_{thigh} and l_{shank} are the length of the thigh and shank, respectively. l_{ankle} is the height of the ankle and l_{waist} is the width between the hips. The spatial vector method[19] is used to solve our rigid body dynamics problem. When using this method, the frame, expressing the variables, must be specified. In this paper, left superscripts denote the reference frame, and variables with $\hat{}$ superscripts denote spatial variables which are vectors with six elements. The floating base coordinate frame Σ_R is located at the center of the pelvis, and the fixed base coordinate frame Σ_W, also known as the world frame, is fixed with the ground. The floating base is the root of this model, which is built by using a kinematic tree. Six virtual joints are introduced between Σ_W and Σ_R. The first three joints are translations in the x, y and z directions, and the next three are successive rotations about the x, y and z axes in that order. These virtual joints are used to express the location of this model in the world frame. $q_r \in R^{6\times1}$ represents the positions and angles of these virtual joints. The dynamics of this model with floating base is

$$M(q)\ddot{q} + C(q, \dot{q}) = \tau, \tag{1}$$

where $\tau = [\tau_r\ \tau_{rl}\ \tau_{ll}]^T$, $M(q) \in R^{18\times18}$ is the joint space inertia matrix, $C(q, \dot{q}) \in R^{18\times1}$ is a vector containing the Coriolis, centrifugal and gravitational terms, and $q = [q_r\ q_{rl}\ q_{ll}]^T$. $\tau_r \in R^{6\times1}$ is torque input of the the six virtual joints. It usually equals to zero because the virtual joints do not introduce constraints. $\tau_{rl} \in R^{6\times1}$ and $\tau_{ll} \in R^{6\times1}$ are torque inputs of the right leg and left leg, respectively.

https://doi.org/10.1017/S0263574714002057 Published online by Cambridge University Press

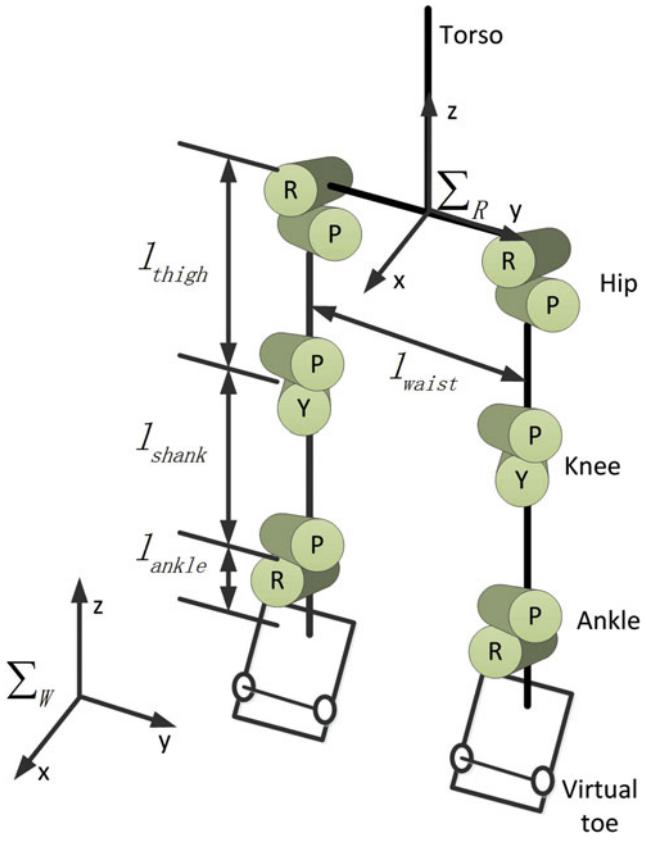

Fig. 3. A bipedal model.

When the foot contacts the ground, both the velocity and acceleration of the foot are zero with respect to ground. The velocity equal to zero is useless when deriving the controller, so it is omitted. The kinematic constraints on acceleration are described by

$$\frac{d}{dt}\left({}^{W}J_{rf}\dot{q}\right) = 0 \tag{2}$$

and/or

$$\frac{d}{dt}\left({}^{W}J_{lf}\dot{q}\right) = 0, \tag{3}$$

where ${}^{W}J_{rf} \in R^{6\times 18}$ is the Jacobian from the right foot coordinate frame to Σ_W and ${}^{W}J_{lf} \in R^{6\times 18}$ is the Jacobian from the left foot to Σ_W. The dynamics of this model with kinematic constraints is written as

$$M(q)\ddot{q} + C(q,\dot{q}) = \tau + {}^{W}J_{rf}^{T}\,{}^{W}\hat{f}_{rf} + {}^{W}J_{lf}^{T}\,{}^{W}\hat{f}_{lf}, \tag{4}$$

where ${}^{W}\hat{f}_{rl} \in R^{6\times 1}$ is the external force acting on the right foot and expressed in Σ_W, and ${}^{W}\hat{f}_{lf} \in R^{6\times 1}$ is that of the left foot.

We introduce some variables, which will be used later. ${}^{W}p_r = [{}^{W}\theta_r\ {}^{W}l_r]^T = [\theta_x\ \theta_y\ \theta_z\ l_x\ l_y\ l_z]^T$ is the attitude and position of Σ_R with respect to Σ_W expressed in Σ_W; and ${}^{R}\hat{v}_r = [{}^{R}\omega_r\ {}^{R}v_r]^T = [\omega_x\ \omega_y\ \omega_z\ v_x\ v_y\ v_z]^T$ is the spatial velocity of the floating base expressed in Σ_R. ${}^{W}p_r$ is used to obtain the coordinate transformation matrix ${}^{R}X_W$, which transforms spatial velocities, accelerations and forces from Σ_W to Σ_R.

https://doi.org/10.1017/S0263574714002057 Published online by Cambridge University Press

The relationship between the spatial acceleration of the floating base ${}^{W}\hat{a}_r$ and the angular acceleration of the virtual joints is

$$\ddot{q}_r = {}^{W}J_R^{-1}\left({}^{W}\hat{a}_r - {}^{W}\dot{J}_R\dot{q}_r\right), \tag{5}$$

where ${}^{W}J_R$ is the Jacobian from Σ_R to Σ_W.

With the kinematic constraints (2) and/or (3), the relationships between $\ddot{q}_{rl}$, $\ddot{q}_{ll}$ and $\ddot{q}_r$ are

$$\ddot{q}_{rl} = {}^{W}J_{rf2}^{-1}\left(-{}^{W}\dot{J}_{rf}\dot{q} - {}^{W}J_{rf1}\ddot{q}_r\right), \tag{6}$$

and

$$\ddot{q}_{ll} = {}^{W}J_{lf3}^{-1}\left(-{}^{W}\dot{J}_{lf}\dot{q} - {}^{W}J_{lf1}\ddot{q}_r\right), \tag{7}$$

respectively, where ${}^{W}J_{rf} = [{}^{W}J_{rf1}\ {}^{W}J_{rf2}\ {}^{W}J_{rf3}]$ and ${}^{W}J_{lf} = [{}^{W}J_{lf1}\ {}^{W}J_{lf2}\ {}^{W}J_{lf3}]$. ${}^{W}J_{rf1}$, ${}^{W}J_{rf2}$, ${}^{W}J_{rf3}$, ${}^{W}J_{lf1}$, ${}^{W}J_{lf2}$ and ${}^{W}J_{lf3} \in R^{6\times 6}$.

The relationship between spatial acceleration and conventional acceleration is

$${}^{W}\hat{a}_r = {}^{R}X_W^{-1}\left(a^c - \begin{bmatrix} 0_{3\times 1} \\ {}^{R}\omega_r \times {}^{R}v_r \end{bmatrix}\right), \tag{8}$$

where $a^c = [{}^{R}\dot{\omega}_r\ {}^{R}\dot{v}_r]^T$ is the conventional acceleration of the floating base in Σ_R.

As long as a^c is known, $\ddot{q}$ can be calculated by (5), (6), (7) and (8). Then, joint torques are derived by inverse dynamics.

3.2. Desired external forces

As mentioned in part A of this section, there are six virtual joints between the floating base and the ground. To compute the desired external forces that accelerate the robot with the desired accelerations, the model with these virtual joints can be treated as a fixed base model without external forces, with the ground as the fixed base. So the joint torques are calculated by (1). τ_r is rarely equal to zero in this case. It results from the desired external forces acting on the floating base. The desired external forces are derived through

$${}^{W}\hat{f}_{ext} = {}^{W}J_R^{-T}\tau_r, \tag{9}$$

where ${}^{W}\hat{f}_{ext}$ is the desired total external force. It is provided by the supporting foot, one foot in SSP and two feet in DSP.

3.3. Control in operational space

The desired acceleration a^c is given by

$$a^c = K_p\,{}^{R}R_W\left({}^{W}p_r^{ref} - {}^{W}p_r\right) + K_d\left({}^{R}R_W\,{}^{W}v_r^{ref} - {}^{R}\hat{v}_r\right), \tag{10}$$

where K_p and K_d are PD gain matrices, ${}^{R}R_W = \left[\begin{smallmatrix} I_{3\times 3} & 0_{3\times 3} \\ 0_{3\times 3} & R^{-1} \end{smallmatrix}\right]$, R is the posture matrix of the floating base in Σ_W, ${}^{W}p_r^{ref}$ and ${}^{W}v_r^{ref}$ are the desired position and velocity of the floating base, respectively.

Similarly, given a desired trajectory to the swinging foot, its conventional accelerations can be calculated.

Because $\ddot{q}$ and ${}^{W}\hat{f}_{ext}$ are obtained through (8) and (9), joint torques are calculated by

$$\begin{bmatrix} 0_{6\times 1} \\ \tau_{rl} \\ \tau_{ll} \end{bmatrix} = M\ddot{q} + C - {}^{W}J_{rf}^{T}K_f\,{}^{W}\hat{f}_{ext} - {}^{W}J_{lf}^{T}(I - K_f)\,{}^{W}\hat{f}_{ext}. \tag{11}$$

K_f is a force distribution matrix, which varies to keep the ZMP of each foot within its own supporting area.

https://doi.org/10.1017/S0263574714002057 Published online by Cambridge University Press

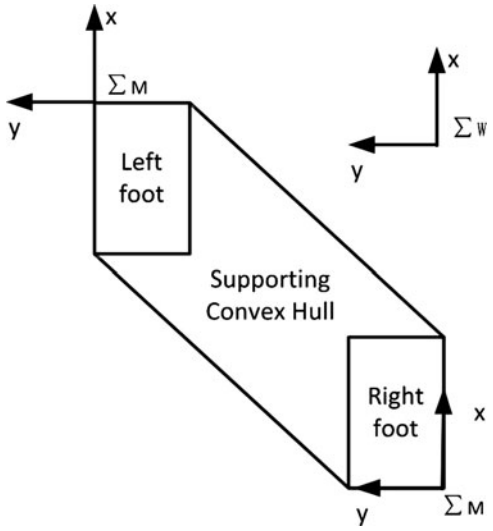

Fig. 4. Supporting convex hull.

3.4. Acceleration optimization

In the last two subsections, the desired acceleration is obtained by (10) and its corresponding external force is obtained by (9). However, the desired external forces are not always equal to the GRFs because the biped model is an underactuated system and the SCH, which is shown in Fig. 4, is limited. If we want to break the kinematic contact constraint when it is necessary, the first step is to confine the desired external forces according to their constraints; otherwise, breaking the kinematic contact constraint is not controllable because the foot rotation around the toe or heel, the slipping and the foot leaving the ground are not predictable. Thus, if the desired external forces do not satisfy these constraints, their corresponding desired accelerations are optimized by quadratic programming.

First, the relationship between the accelerations of the floating base and their corresponding external forces is established. After that, the acceleration optimization will be presented.

From (4), we get

$$M_{11}\ddot{q}_r + M_{12}\ddot{q}_{rl} + M_{13}\ddot{q}_{ll} + C_1 = {}^{W}J_{M1}^{T}\,{}^{M}X_{W}^{T}\,{}^{M}\hat{f}_m, \tag{12}$$

where M_{11}, M_{12} and $M_{13} \in R^{6\times 6}$ and $[M_{11}\ M_{12}\ M_{13}]$ are the elements of the first six lines of $M(q)$. C_1 represents the first six elements of $C(q, \dot{q})$. ${}^{M}X_{W}$ is the coordinate transformation matrix from Σ_W to frame Σ_M (See Fig. 4.). Σ_M is located where the GRFs provide the maximum or minimum accelerations. Its location is selected according to the SCH. Σ_M is established on the edge of the foot. ${}^{M}\hat{f}_m$ is the desired external force expressed in this frame.

According to our previous work,[20] $\ddot{q}$ is a function of a^c, a_{rf} and a_{lf}. a_{rf} and a_{lf} are the spatial accelerations of the swinging foot in Σ_R. Omitting its derivation, (12) can be rewritten as

$$Ua^c + V = {}^{M}\hat{f}_m, \tag{13}$$

where $U = U(q, \dot{q})$ and $V = V(q, \dot{q}, a_{rf}\ or\ a_{lf})$. $U \in R^{6\times 6}$ and $V \in R^{6\times 1}$.

${}^{M}\hat{f}_m$ is a spatial vector which has six elements, ${}^{M}\hat{f}_m = [n_{Mx}\ n_{My}\ n_{Mz}\ f_x\ f_y\ f_z]^T$. The force constraints, mentioned above, can be further understood through the following inequalities.

- $f_z > 0$. The ground can only push the feet.
- $\frac{f_x}{f_z} < \frac{\mu}{\sqrt{2}}$ and $\frac{f_y}{f_z} < \frac{\mu}{\sqrt{2}}$. No slipping occurs. μ is the coefficient of friction.
- $n_{My} \geq or \leq 0$ guarantees the desired ZMP within the SCH in the x direction. Choosing $\geq$ or $\leq$ depends on where the coordinate frame is. For instance, if the frame is at the front side of the SCH, $\geq$ is selected; if the frame is at the back side of the SCH, $\leq$ is selected.

https://doi.org/10.1017/S0263574714002057 Published online by Cambridge University Press

- $n_{Mx} \geq or \leq 0$ guarantees the desired ZMP within the SCH in the y direction. If the frame is at the left side of the SCH, $\leq$ is selected; if the frame is at the right side of the SCH, $\geq$ is selected.

There are two ${}^{M}\hat{f}_m$, which are used to constrain the desired accelerations. The inequality equation is

$$A \cdot a^c_{act} \leq b, \tag{14}$$

where $A \in R^{10\times 3}$ and $b \in R^{10\times 1}$ are functions of U and V, respectively. Each of the five inequalities is derived from the constraints on each ${}^{M}\hat{f}_m$. a^c_{act} is the actual acceleration which should satisfy its constraints. Every element in A and b is a function of the elements in U and V. A and b can only be expressed as implicit functions of U and V.

The cost function is

$$f(a^c_{act}) = W_t \cdot ||a^c_{act} - a^c_{des}||, \tag{15}$$

where a^c_{des} is the desired acceleration obtained by (10), and W_t is a weight matrix.

Finally, the optimal accelerations a^c_{opt} is obtained by

$$a^c_{opt} = \min_{a^c_{act}} f(a^c_{act}),\ s.t.\ A \cdot a^c_{act} \leq b. \tag{16}$$

a^c_{opt} is used instead of a^c_{des} to perform inverse dynamics.

Whether the kinematic contact constraints are broken, the controller outputs joint torques that drive the model to move. According to the inequalities before (14), when the desired ZMP is within the SCH, the torques let the foot maintain contact with the ground. When the desired ZMP exceeds the SCH, the torques allow the foot to rotate. Thus, the ZMP can be purposely predefined into the toe so that the foot rotates around it.

4. Pattern Generation

In the last section, we have presented a controller, which enables our robot to rotate its supporting foot around its toe. This section presents a pattern generation approach, which can predefine a moving ZMP so that the ZMP can be planned in the toe.

4.1. Extended linear inverted pendulum model

In the conventional LIPM, it is assumed that the mass of the robot can be lumped to the CoM which is supported by a massless telescopic limb. When the CoM is kept at a constant height, its motion in the frontal direction is independent of the motion in the lateral direction. With the assumption ${}^{W}z_{com} = Z_{com}$, the dynamics equations are given as follows:

$${}^{W}\ddot{x}_{com} - \frac{g}{Z_{com}}{}^{W}x_{com} = -\frac{g}{Z_{com}}{}^{W}x_{zmp}, \tag{17}$$

$${}^{W}\ddot{y}_{com} - \frac{g}{Z_{com}}{}^{W}y_{com} = -\frac{g}{Z_{com}}{}^{W}y_{zmp}, \tag{18}$$

where g is the gravity acceleration, $[{}^{W}x_{com}\ {}^{W}y_{com}\ {}^{W}z_{com}]^T$ is the CoM position in Σ_W, and $[{}^{W}x_{zmp}\ {}^{W}y_{zmp}\ 0]^T$ is the ZMP position in Σ_W.

Because the motions in the sagittal plane and lateral plane are independent from each other, we will focus on the motion in the sagittal plane because the motion in the lateral plane can be obtained similarly.

LIPM sets ${}^{W}x_{zmp}$ to zero to simplify its dynamics equation. In this case, (17) and (18) become easier and we can obtain an analytic expression of the CoM motion.[7] When the ZMP is fixed in the middle of the sole for high stability, the sole is always kept horizontal when the robot walks. It is hard for the robot to walk fast with feet parallel to the ground all the time.

https://doi.org/10.1017/S0263574714002057 Published online by Cambridge University Press

To make the ZMP adjustable, we do not set the ZMP to zero when using the LIPM. The CoM state is obtained by

$$\begin{bmatrix} {}^{W}x_{com}(t) \\ T_c\,{}^{W}v_{xcom}(t) \end{bmatrix} = \begin{bmatrix} C_t & S_t \\ S_t & C_t \end{bmatrix} \begin{bmatrix} {}^{W}x_{com}(0) \\ T_c\,{}^{W}v_{xcom}(0) \end{bmatrix} - \frac{1}{T_c} \begin{bmatrix} \int_0^t S_t\,{}^{W}\overline{p}_{xzmp}(\sigma)d\sigma \\ \int_0^t C_t\,{}^{W}\overline{p}_{xzmp}(\sigma)d\sigma \end{bmatrix}, \tag{19}$$

where $[{}^{W}x_{com}(t) \quad {}^{W}v_{xcom}(t)]^T$ and $[{}^{W}x_{com}(0) \quad {}^{W}v_{xcom}(0)]^T$ represent states at the moment t and the initial moment, respectively. $T_c = \sqrt{Z_{com}/g}$. S_t and C_t represent $sinh(t/T_c)$ and $cosh(t/T_c)$, respectively. ${}^{W}\overline{p}_{xzmp}(\sigma)$ represents the ZMP trajectory and ${}^{W}\overline{p}_{xzmp}(\sigma) = {}^{W}p_{xzmp}(t-\sigma)$.

Briefly, we use a uniform form to express ZMP trajectories. Assume the ZMP moves from ${}^{W}S_{xzmp}$ to ${}^{W}S_{xzmp} + {}^{W}L_{xzmp}$ during $[t_1, t_2]$. Then, the ZMP trajectory is given as

$${}^{W}\overline{p}_{xzmp}(t) = {}^{W}K_{xzmp} \cdot (t - t_1) + {}^{W}S_{xzmp},\ t_1 \le t \le t_2, \tag{20}$$

where ${}^{W}K_{xzmp} = {}^{W}L_{xzmp}/(t_2 - t_1)$.

Substitute (20) into (19), the CoM state in the forward direction is obtained by

$$\begin{bmatrix} {}^{W}x_{com}(t) \\ T_c\,{}^{W}v_{xcom}(t) \end{bmatrix} = \begin{bmatrix} C_t & S_t \\ S_t & C_t \end{bmatrix} \begin{bmatrix} {}^{W}x_{com}(0) \\ T_c\,{}^{W}v_{xcom}(0) \end{bmatrix} - \frac{1}{T_c} \begin{bmatrix} T_c^2 S_t - T_c t & T_c(C_t - 1) \\ T_c^2(C_t - 1) & T_c S_t \end{bmatrix} \begin{bmatrix} {}^{W}K_{xzmp} \\ {}^{W}S_{xzmp} \end{bmatrix}, \tag{21}$$

where $S_{t/2}$ is $sinh(\frac{t}{2T_c})$.

In (21), the CoM state is a function of the ZMP, which means the ZMP is adjustable and can be set as required.

4.2. Foot placement

Foot placement is very important for stability control. To remain stable, the robot must choose an appropriate location for the swinging foot according to the current CoM state.

First, the CoM velocity at the end of the SSP is predicted according to the current CoM state. Then, foot placement is calculated according to the predicted velocity and the desired one. Suppose the desired velocity of the CoM is V_{des}, which is the CoM velocity when the swinging foot touches the ground.

Starting with the current CoM state, the CoM state at moment T is obtained by

$$\begin{aligned} \begin{bmatrix} {}^{W}x_{com}(T) \\ T_c\,{}^{W}v_{xcom}(T) \end{bmatrix} &= \begin{bmatrix} C_{T-t} & S_{T-t} \\ S_{T-t} & C_{T-t} \end{bmatrix} \begin{bmatrix} {}^{W}x_{com}(t) \\ T_c\,{}^{W}v_{xcom}(t) \end{bmatrix} \\ &\quad - \frac{1}{T_c} \begin{bmatrix} T_c^2 S_{T-t} - T_c(T-t) & T_c(C_{T-t} - 1) \\ T_c^2(C_{T-t} - 1) & T_c S_{T-t} \end{bmatrix} \begin{bmatrix} {}^{W}K_{xzmp} \\ {}^{W}S_{xzmp} + {}^{W}K_{xzmp} * t \end{bmatrix}. \end{aligned} \tag{22}$$

Using the velocity equation in (22), the starting point of the ZMP position in Σ_R is

$$\begin{aligned} {}^{R}x_S &= {}^{W}S_{xzmp} - {}^{W}x_{com}(0) \\ &= -T_c/S_t(V_{des} - C_t T_c\,{}^{W}v_{xcom}(0) + (C_t - 1)^{W}K_{xzmp}). \end{aligned} \tag{23}$$

Suppose the position of the ZMP starting point in the ankle coordinate frame is ${}^{A}x_S$. Then, the desired position of the ankle of the swinging foot in Σ_R is

$${}^{R}x_{ankle} = {}^{R}x_S - {}^{A}x_S. \tag{24}$$

https://doi.org/10.1017/S0263574714002057 Published online by Cambridge University Press

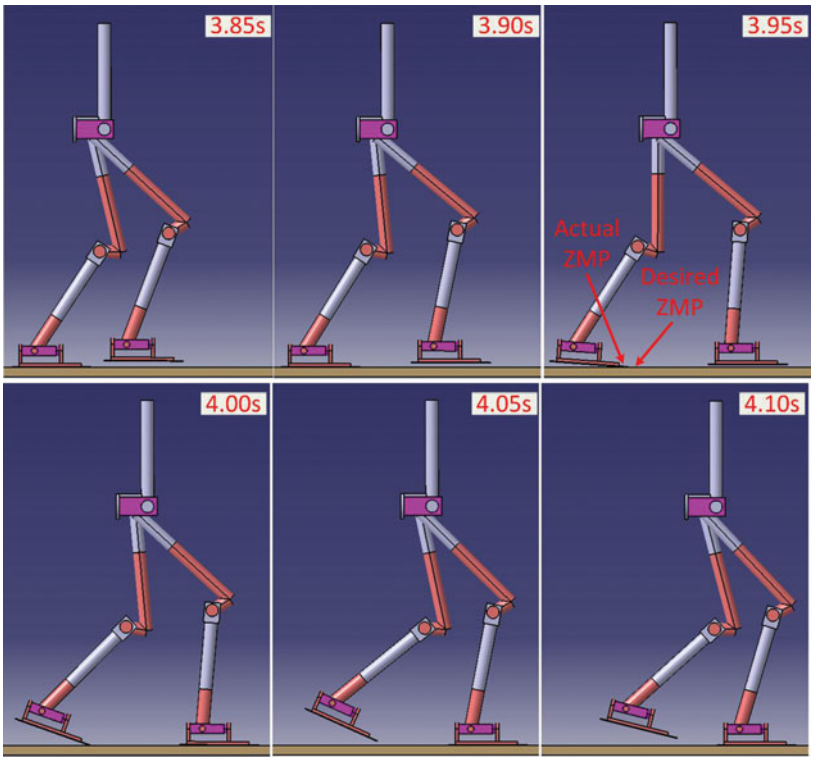

Fig. 5. Screenshots of walking.

When the supporting leg becomes the swinging leg, the position and velocity of the ankle in Σ_R are known. The target position is computed according to (22), (23) and (24). Finally, cubic spline interpolation is used to generate the trajectories for the swinging leg.

The mass of the torso is more than 70% of the total mass of the robot. To simplify, we assume the CoM is fixed on the torso, which means the desired CoM trajectory is the desired torso trajectory.

5. Simulation

The biped model is built in a commercial simulator, LMS Virtual Lab. The main physical parameters are set in accordance with the real robot. $l_{thigh} = 0.39\,\text{m}$, $l_{shank} = 0.38\,\text{m}$, $l_{ankle} = 0.05\,\text{m}$, $l_{waist} = 0.18\,\text{m}$. The mass of the torso is 69 kg and the total mass of the model is approximately 97 kg. The peak torque of the joint is limited in accordance with its actuators. The peak torques of the hip, knee and ankle in the pitch direction are 226 Nm, 293 Nm and 202 Nm, respectively. We use a contact model,[21] which is closer to the real contact than the spring-damper model. We derive our method in 3D. However, in this paper we fix the torso in the sagittal plane and only focus on the motion in that plane. We use our method as the following steps. First, because the CoM is assumed to be fixed on the torso, the desired position and velocity of the torso are computed by (21), and the desired position of the swinging foot is computed by (24). Second, we can measure the state of the model, which consists of the position and velocity of the torso, ${}^W p_r$ and ${}^W \hat{v}_r$, and the angle and angular velocity of the joints, q and $\dot{q}$. Thus, the desired acceleration of the torso a^c_{des} can be computed by (10) and desired acceleration of the swinging leg can be calculated by the PD control algorithm. Third, the optimal acceleration of the torso a^c_{opt} is obtained by (16) and then $\ddot{q}$ is derived. Fourth, the external forces ${}^W \hat{f}_{ext}$ applied to the feet are computed by (1) and (9). Finally, the joint torques applied to the model are computed by (11) according to $\ddot{q}$ and ${}^W \hat{f}_{ext}$ which are already known.

The desired velocity is 1.1 m/s. The desired period of SSP is 0.5 s and the period of DSP is 0.05 s. States 3 and 6 are event triggered, so the actual period of SSP may be a little bit longer or shorter than 0.5 s because the swinging foot may contact the ground earlier or later than the desired period of SSP. The torso is kept at a constant height.

https://doi.org/10.1017/S0263574714002057 Published online by Cambridge University Press

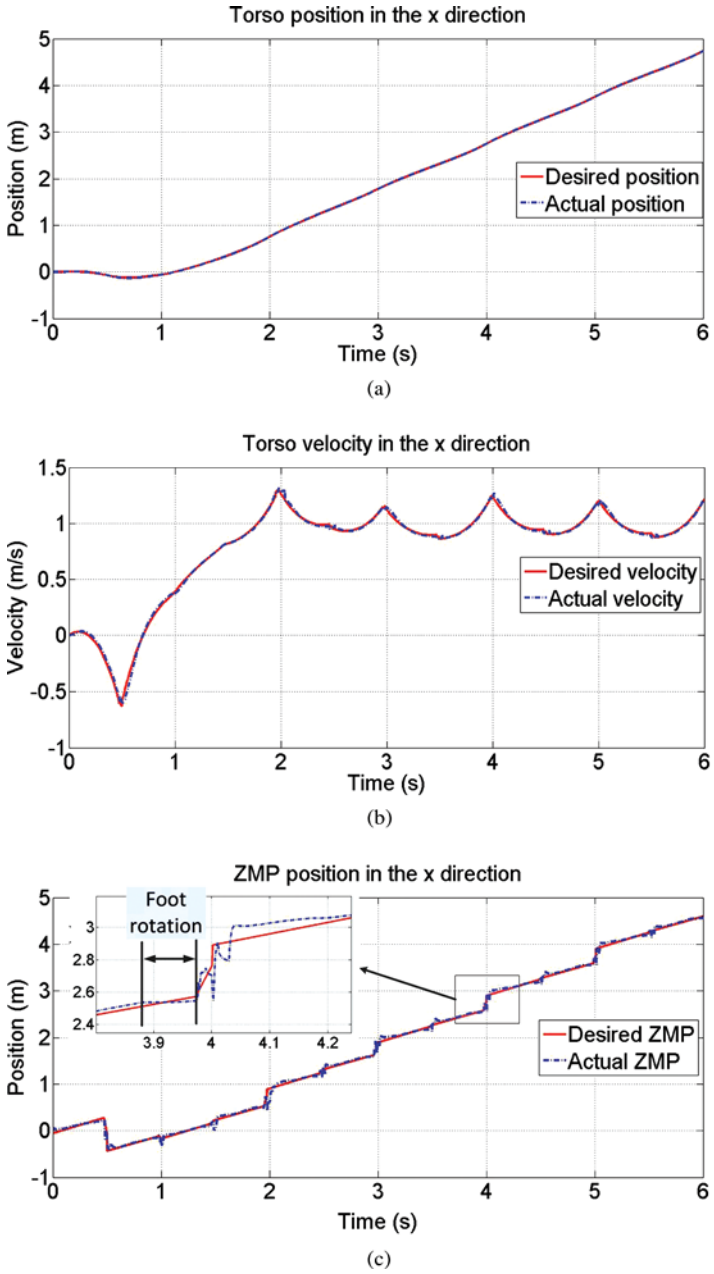

Fig. 6. The torso motion in the forward direction in the world frame. To initiate forward movement, the robot first steps backward. It reaches the desired velocity in approximately 2 s and then keeps walking at an average speed of 1.1 m/s.

The desired ZMP is shifted from the heel to the toe in SSP and from the toe of the rear foot to the heel of the front foot in DSP. So the desired ZMP is in the toe of the supporting foot at the end of SSP. The robot starts to walk from a standing start. Figure 5 shows the screenshots of the robot walking from 3.85 s. to 4.10 s. Moment 3.95 s. is in SSP, and at this moment the rear leg is the supporting leg and its foot rotates. Moment 4.00 s. is in DSP, and at this moment the fore leg becomes the supporting leg and we do not care whether the rear leg (swinging leg) breaks the contact constraint or not. Therefore, there is an obvious period when the supporting foot rotates around its toe before the swinging foot contacts the ground. Figure 6(a) and (b) show the position and velocity of the torso in the world frame, respectively. They are tracking their references well. From Fig. 6(c), we can see that the actual ZMP is constant for approximately 0.1 s. after moment 3.95 s., which means the ZMP is located at the front edge for a while; during this period, the kinematic contact constraint breaks and

https://doi.org/10.1017/S0263574714002057 Published online by Cambridge University Press

the foot rotates around its toe. The foot placement varies according to the CoM state and the desired walking velocity.

6. Conclusion and Future Work

To further increase walking speed, this study has presented a method to realize foot rotation by breaking the kinematic contact constraint. The inverse dynamics controller enables the biped model to break the constraint when the desired ZMP is in the toe. LIPM is extended to make its ZMP adjustable so that the ZMP can be set as required. To imitate the CoP of human walking, the ZMP is predefined from the heel to the toe so that the supporting foot rotates around its toe for a while at the end of SSP. The effectiveness of the proposed method was demonstrated by simulation.

In this paper, we focus on the foot rotation of the supporting leg, which is called toe-off. The heel strike is also useful to increase walking speed, and it affects the impact when the swinging foot contacts the ground. From Fig. 6(c), we can see that this impact was not eliminated because the actual ZMP did not track its reference well in the DSP. In the future, we will extend our work by combining toe-off with heel-strike.

Acknowledgment

This work was supported by the National Natural Science Foundation of China under Grants 61320106012, 61375103, 61273348 and 61175077, the 863 Project under Grant 2014AA041602, "111 Project" under Grant B08043, and Beijing Municipal Science and Technology Project.

References

1. Y. Sakagami, R. Watanabe, C. Aoyama, S. Matsunaga, N. Higaki and Fujimura, "The Intelligent ASIMO: System Overview and Integration," *Proceedings of the IEEE/RSJ International Conference Intelligent Robots and Systems* (2002) pp. 2478–2483.
2. K. Kaneko, F. Kanehiro, S. Kajita, H. Hirukawa, T. Kawasaki, M. Hirata, K. Akachi and T. Isozumi, "Humanoid Robot HRP-2," *Proceedings of the IEEE International Conference on Robotics and Automation* (2004) pp. 1083–1090.
3. Z. Yu, G. Ma and Q. Huang, "Modeling and design of a humanoid robotic face based on an active drive points model," *Adv. Robot.* **28**(6), 379–388 (2014).
4. J. Pratt and B. Krupp, "Design of a Bipedal Walking Robot," *Prcoeedings of SPIE* (2008) pp. 69621F–69621F-13.
5. Boston Dynamics. *http://www.bostondynamics.com/robot_petman.html*
6. I. Kato, S. Ohteru, H. Kobayashi, K. Shirai, A. Uchiyama, "Information-Power Machine with Senses and Limbs," *Proceedings CISM-IFToMM Symposium on Theory and Practice of Robots and Manipulators* (1973) pp. 12–24.
7. S. Kajita, F. Kanehiro, K. Kaneko, K. Yokoi and H. Hirukawa, "The 3D Linear Inverted Pendulum Mode: A Simple Modeling for a Biped Walking Pattern Generation," *Proceedings of the IEEE/RSJ International Conference Intelligent Robots and Systems* (2001) pp. 239–246.
8. Q. Huang, K. Yokoi, S. Kajita, K. Kaneko, H. Arai, N. Koyachi and K. Tanie, "Planning walking patterns for a biped robot," *IEEE Trans. Robot. Autom.* **17**(3) (2001).
9. H. Lim, Y. Kaneshimat and A. Takanishi, "Online walking pattern generation for biped humanoid robot with trunk," *Proceedings of the IEEE International Conference Robotics and Automation* (2002) pp. 3111–3116.
10. S. Cuccurullo (ed.), *Gait Analysis - Physical Medicine and Rehabilitation Board Review* (Demos Medical Publishing, 2004).
11. K. Nishiwaki, S. Kagami, Y. Kuniyoshi, M. Inaba and H. Inoue, "Toe Joints that Enhance Bipedal and Full-Body Motion of Humanoid Robots," *Proceedings of the IEEE International Conference on Robotics and Automation* (2002) pp. 3105¤C3110.
12. D. Tlalolini, C. Chevallereau and Y. Aoustin, "Human-like walking: Optimal motion of a bipedal robot with Toe-Rotation motion," *IEEE Trans. Mechatronics* **16**(2) (Apr. 2011).
13. C. K. Ahn, M. C. Lee and S. J. Go, "Development of a biped robot with Toes to improve gait pattern," *Proceedings of the IEEE/ASME International Conference on Advanced Intelligent Mechatronics* (2003) pp. 729–734.
14. Y. Ogura, K. Shimomura, H. Kondo, A. Morishima, T. Okubo, S. Momoki, H. Lim and A. Takanishi, "Human-like walking with knee stretched, Heel-contact and Toe-off motion by a humanoid robot," *Proceedings of the IEEE/RSJ International Conference on Intelligent Robots and Systems* (2006) pp. 3976–3981.
15. Q. Huang, Z. Yu, W. Zhang, W. Xu and X. Chen, "Design and similarity evaluation on humanoid motion based on human motion capture," *Robotica* **28**, 737–745 (2010).

16. F. L. Moro, N. G. Tsagarakis and D. G. Caldwell, "A Human-like Walking for the COmpliant huMANoid COMAN based on CoM Trajectory Reconstruction from Kinematic Motion Primitives," *Proceedings of the IEEE/RSJ International Conference on Humanoid Robots* (2011) pp. 364–370.
17. S. Coros, P. Beaudoin and M. van de Panne, "Generalized Biped Walking Control," *Proceedings of the ACM SIGGRAPH* (2010).
18. Q. Huang and Y. Nakamura, "Sensory reflex control for humanoid walking," *IEEE Trans. Robot.* **21**(5) (Oct. 2005).
19. R. Featherstone, "Spatial vector algebra," [Online] (2010). Available: *http://users.cecs.anu.edu.au/∼roy/spatial/*
20. X. Chen, Q. Huang, Z. Yu and Y. Lu, "Robust push recovery by whole-body dynamics control with extremal accelerations," *Robotica* **32**(3), 467–476 (2014).
21. H. Han, T. Kim and T. Park, "Tolerance Analysis of a Spur Gear train," *Proceedings of 3rd DADS Korean User's Conference* (1987) pp. 61–81.

https://doi.org/10.1017/S0263574714002057 Published online by Cambridge University Press